BRAIN CONNECTIVITY
Volume 9, Number 5, 2019

DOI: 10.1089/brain.2018.0653

Children with Autism Spectrum Disorder Demonstrate Regionally Specific Altered Resting-State Phase–Amplitude Coupling

Russell G. Port,[1,2] Marissa A. Dipiero,[2] Matthew Ku,[2] Song Liu,[2] Lisa Blaskey,[2,3] Emily S. Kuschner,[1,2] J. Christopher Edgar,[2,4] Timothy P.L. Roberts,[2,4] and Jeffrey I. Berman[2,4]

Abstract

Studies suggest that individuals with autism spectrum disorder (ASD) exhibit altered electrophysiological alpha to gamma phase–amplitude coupling (PAC). Preliminary reports with small samples report conflicting findings regarding the directionality of the alpha to gamma PAC alterations in ASD. The present study examined resting-state activity throughout the brain in a relatively large sample of 119 children with ASD and 47 typically developing children. Children with ASD demonstrated regionally specific abnormalities in alpha to low-gamma PAC, with increased alpha to low-gamma PAC for a central midline source and decreased PAC at lateral sources. Group differences in local gamma-band power did not account for the regional group differences in alpha to low-gamma PAC. Moreover, local alpha power did not significantly modulate alpha to low-gamma PAC estimates. Finally, PAC estimates were correlated with Social Responsiveness Scale (SRS) indicating clinical relevance of the PAC metric. In conclusion, alpha to low-gamma PAC alterations in ASD demonstrate a heterogeneous spatial profile consistent with previous studies and were related to symptom severity.

Keywords: alpha; autism spectrum disorder; gamma; MEG; PAC; resting state

Introduction

Autism spectrum disorder (ASD) is a neurodevelopmental disorder characterized by social and communication impairments as well as restricted and/or stereotyped behaviors (American Psychiatric Association, 2013). ASD may arise from imbalances between excitatory and inhibitory neurosignaling (E/I imbalance) (Hussman, 2001; Rubenstein and Merzenich, 2003). Evidence for E/I imbalances in ASD has been observed clinically (Fatemi et al., 2009; Gaetz et al., 2014; Harada et al., 2011), as well as in preclinical models that recapitulate key aspects of ASD (Gandal et al., 2012; Gogolla et al., 2009; Port et al., 2017b).

Indirect evidence for E/I imbalance in ASD also arises from electrophysiological studies of ASD. In particular, gamma-band (30–100 Hz; gamma) electrophysiological activity is known to be highly reliant on the $GABA_A$ receptor time constant (Traub et al., 1996) and sensitive to the balance of excitatory and inhibitory neurosignaling (Traub et al., 1998). Electroencephalography (EEG) and magnetoencephalography (MEG) studies have observed gamma-band alterations in individuals with ASD (Edgar et al., 2015c; Grice et al., 2001; Port et al., 2016; Wilson et al., 2007).

Local hyperconnectivity in conjunction with long-range hypoconnectivity has been hypothesized in ASD (Belmonte et al., 2004; Just et al., 2004; Wass, 2011). Gamma-band activity is thought to arise from local circuit interactions as opposed to regional activity (Buzsaki and Wang, 2012). Long-range connectivity conveyed by white matter networks may be indexed by lower frequency activity (Kopell et al., 2014), with alterations to low-frequency oscillatory electrophysiological activity demonstrated in ASD (Cornew et al., 2012; Edgar et al., 2015a; Tierney et al., 2012). Abnormal development of long-range white matter structures and network architecture in ASD has also been observed using diffusion-weighted magnetic resonance imaging and tractography (Berman et al., 2016; McLaughlin et al., 2018; Roberts et al., 2013).

A recent development in the study of oscillatory electrophysiological activity is the examination of cross-frequency coupling (CFC), and in particular phase–amplitude coupling

[1]Department of Psychiatry, Perelman School of Medicine, University of Pennsylvania, Philadelphia, Pennsylvania.
[2]Department of Radiology, Lurie Family Foundations MEG Imaging Center, Children's Hospital of Philadelphia, Philadelphia, Pennsylvania.
[3]Department of Pediatrics, Center for Autism Research, The Children's Hospital of Philadelphia, Philadelphia, Pennsylvania.
[4]Department of Radiology, Perelman School of Medicine, University of Pennsylvania, Philadelphia, Pennsylvania.

(PAC) (Canolty et al., 2006; Osipova et al., 2008). CFC denotes the phenomenon where a higher frequency signal is modulated or gated by a lower frequency signal. PAC, a form of CFC, examines the extent to which the amplitude of a higher frequency signal is modulated by the phase of a concomitant lower frequency signal (Canolty et al., 2006; Osipova et al., 2008). A few studies have investigated PAC in ASD. Khan et al. (2013) observed decreased task-induced relative alpha to gamma PAC in ASD. A follow-up study determined that the decreased task-induced relative alpha to gamma PAC in ASD was only present for adolescent, but not child, participants (Mamashli et al., 2018). Decreased PAC in ASD has also been observed using simple grating stimuli (Seymour et al., 2018). Recently, our group observed greater alpha to low-gamma resting-state (RS) PAC in children with ASD than their typically developing (TD) counterparts when examining a single posterior midline regional source (Berman et al., 2015).

The current study expands on our initial efforts (Berman et al., 2015) by assessing PAC across the entire cerebral cortex as well as increasing the sample size. To provide insight into any observed potential RS PAC alterations, RS power was additionally investigated within canonical frequency bands. It was hypothesized that (1) individuals with ASD would demonstrate greater posterior alpha to gamma PAC compared with their TD counterparts across regional sources in concordance with Berman et al. (2015), and (2) individuals with ASD would demonstrate increased RS alpha- and gamma-band power over posterior and temporal regions compared with their TD counterparts in accordance with Cornew et al. (2012).

Materials and Methods

Participants

Participants included 128 children with ASD and 50 TD children. Data from 48 of these subjects (26 children with ASD and 22 TD children) were previously reported in a primarily methods study where PAC results were reported for a single midline posterior regional source (Berman et al., 2015). This study expands on the previous study by examining a total of 15 regional sources across the cerebral cortex. In addition, a subset of the RS power spectrum data was reported in Cornew et al. (2012).

Clinical assessments were performed by a licensed child psychologist with expertise in ASD. Children with ASD had a prior diagnosis, typically made by an expert clinician in the Children's Hospital of Philadelphia's (CHOP's) Regional Autism Center or, more rarely, by community providers. An abbreviated diagnostic battery confirmed the original diagnosis in the ASD group and ruled out ASD in the TD children. Specifically, diagnostic classification was made using the Autism Diagnostic Observation Schedule (ADOS/ADOS-2) and parent report on the Social Communication Questionnaire (SCQ) (Lord et al., 2000, 2012; Rutter et al., 2003). Dimensional symptom severity indices were obtained by parent report on the Social Responsiveness Scale (SRS/SRS-2) (Constantino and Gruber, 2012) and from the ADOS Calibrated Severity Score metric (Gotham et al., 2009). The parent-completed Autism Diagnostic Interview-Revised (ADI-R) (Le Couteur et al., 2003) was administered for rare participants who entered the study without a formal ASD diagnosis made by an expert clinician (e.g., ASD educational classification only) and for any child with a prior ASD diagnosis for whom a diagnostic discordance existed. To rule out global cognitive delay, all subjects scored at or above the second percentile (SS >70) on at least one index of verbal or nonverbal intellectual functioning from the Wechsler Intelligence Scale for Children-fourth or fifth editions (WISC-IV/WISC-V) (Wechsler, 2003, 2014). The WISC General Ability Index (GAI) served as a measure of overall intellectual functioning. TD-specific inclusion criteria included scoring below the cutoff for ASD on the ADOS-2 as well as parent questionnaires. Additional TD-specific exclusion/inclusion criteria included no history of psychiatric disorders and no developmental disorders or first-degree relatives with ASD. All subjects had no known genetic syndromes, neurological disorders, or sensory impairments. The study was approved by the institutional review board and all participants' families provided written informed consent. As indicated by institutional policy, where competent to do so, children older than seven years additionally gave verbal assent to participation.

MEG acquisition

Data were collected using a 275-channel MEG system (VSM MedTech, Inc.). Children were scanned in a supine position and were instructed to lie still with their eyes gently closed during an RS examination that lasted a maximum of 5 min. Three head-position indicator coils were attached to the scalp and foam wedges inserted between the side of the participant's head and the inside of the dewar to ensure immobility. The electro-oculogram (EOG; bipolar oblique, upper right and lower left sites) was collected to ensure that participants' eyes remained closed throughout the 5-min examination. Recording with a bandpass filter (0.03–150 Hz), EOG and MEG signals were digitized at 1,200 Hz with third-order gradiometer environmental noise reduction and downsampled to 500 Hz.

MEG analysis

Participants' raw EOG data were visually examined and MEG epochs contaminated by blinks, saccades, or other significant EOG activity were removed. Participants' MEG data were visually inspected for muscle-related activity, and data containing muscle activity removed. Any additional artifacts were rejected by magnetic field amplitude and sample/sample gradient criteria (amplitude 1,200 fT/cm, gradients 4,800 fT/cm/sample).

As MEG-derived estimates based on scalp indices likely reflect the superposition of activity from multiple brain areas, assessment of functional connectivity is optimally performed in source rather than sensor space (Hoechstetter et al., 2004; Nunez et al., 1997). A source model with 15 regional sources (Fig. 1) was applied using BESA 6.0 (MEGIS Software GmbH). This source modeling yielded two orthogonally orientated time courses for each regional source. The regional sources are not intended to correspond to precise neuroanatomical structures but rather to represent neural activity at coarse spatial resolution and to provide measures of brain activity with better signal separation and with a greater signal-to-noise ratio than would be afforded at the sensor level. The locations of the regional sources in the model are such that

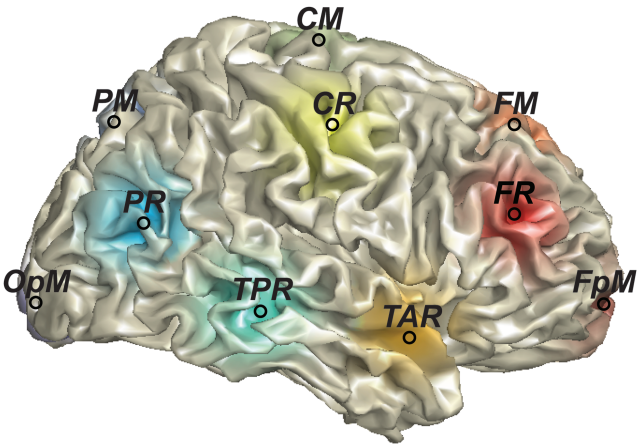

FIG. 1. Regional source locations. RS bandpassed power and PAC were calculated for all sources. The figure shows the locations for FpM, FM, FR, TAR, CM, CR, TPR, PM, PR, and OPM. The left hemisphere contained analogous regional sources, although with region source labels ending with ''L'' instead of ''R.'' CM, central midline; CR, central right; FM, frontal midline; FpM, frontopolar midline; FR, frontal right; OPM, occipito-polar midline; PAC, phase–amplitude coupling; PM, parietal midline; PR, parietal right; RS, resting state; TAR, temporal anterior right; TPR, temporal posterior right. Color images are available online.

there is an approximately equal distance between sources (>3 cm), helping to separate signals originating from different brain regions. RS bandpassed power, as well as PAC, was examined at all 15 regional sources.

RS bandpassed power analysis

In brief, artifact-free RS regional bandpassed power was interrogated for alterations in ASD. To do so, RS power spectral densities were created for each artifact-free epoch of the orthogonally oriented regional time courses and then reconstituted into the corresponding RS bandpassed power. The effects of diagnosis, frequency band, source, age, as well as their interactions on RS bandpassed power, were subsequently examined.

Specifically, all artifact-containing periods of the orthogonally oriented regional time courses were excluded from further analysis, resulting in multiple artifact-free epochs as per each aforementioned time course. Subsequently, only artifact-free epochs longer than 3 sec underwent spectral transformation, to ensure valid calculation of lower frequency activity. Initial RS power spectral densities were then calculated separately for each of the orthogonally oriented regional time course epochs by applying the fast Fourier transformation. The resulting RS power spectral densities for each epoch were then averaged into 1 Hz bins over the 1–120 Hz frequency range. The RS power spectral densities for the two orthogonally oriented time courses within each regional source were then summed to yield the power at a given frequency at that source, in accordance with Cornew et al. (2012).

Power spectral densities were subsequently parsed into canonical spectral bands by averaging across all power values within that band: delta (1–4 Hz), theta (4–8 Hz), alpha (8–12 Hz), beta (15–25 Hz), low gamma (30–60 Hz), and high gamma (60–100 Hz). Linear mixed effects models (LMMs) were subsequently performed in R 3.5.1 (R Core Team, 2018), using the package ''Afex'' (Singmann et al., 2018). Statistical analyses examined RS bandpassed power for the effects of diagnosis, frequency band, source, age, and their interactions. Holm's multiple comparison correction was implemented when *post hoc* interrogating the within source by frequency band pairwise comparison of diagnosis. To aid in the visualization of spectral band power, the estimated marginal means resulting from the diagnosis by region by frequency band interaction, were subsequently used to calculate percent change from TD for each region by frequency band. These percent change values were then plotted onto a template's brain surface (ICBM152 average brain) (Fonov et al., 2009) for each frequency band.

RS PAC analysis

In brief, artifact-free regional PAC estimates were interrogated for alterations in ASD. Subsequently, the maturational trajectories of PAC estimates were investigated both within and across diagnostic groups. Finally, the relationship between regional PAC estimates and ASD symptomology (SRS T-score) was investigated separately for the frequency pairings with the greatest negative and positive effect-size across all group-level location comodulograms.

To obtain location-specific time courses for PAC estimates, the orientation containing the majority of RS activity was identified for each regional dipole. To do so, principal component analysis was applied to the two orthogonal time courses within each region. Subsequently the first component's loading was used to weight the combination of the two orthogonal time courses within each region. These optimal orientated time courses were subsequently used for PAC analyses.

The estimate of PAC published by Tort et al. (2010) was implemented in MATLAB (MathWorks), with the additional use of double sideband (DSB) variable bandwidth filtering for the high-frequency amplitude-modulated signal (Berman et al., 2012, 2015). Each regional source's broadband time-domain source signal was bandpass filtered into two frequency bands of interest: a low-frequency and a high-frequency signal. A Hilbert transform provided the time-varying phase of the low-frequency signal and the time-varying amplitude of the high-frequency signal. In accordance with Port et al. (2019), periods of the high- and low-frequency signals that corresponded to artifact-containing periods in the raw data were subsequently rejected to mitigate artifact contamination. The resulting artifact-free epochs were then concatenated together for the high- and low-frequency signal separately. A composite within-source signal was next formed using the phase time course of the artifact-free low-frequency signal and the amplitude time course of the artifact-free high-frequency signal. This composite signal was then used to measure the dependence of the amplitude of the high-frequency signal on the phase of the low-frequency signal, computed as the modulation index (MI). The MI measures the deviation of the amplitude-phase histogram from a uniform distribution. The underlying assumption is that if the amplitude to phase histogram has a distinct peak, then there is a relationship between the high-frequency signal's amplitude and the low-frequency signal's

phase (Tort et al., 2010). To examine coupling between multiple frequency pairs within each regional location, comodulogram matrices visualize PAC (i.e., MI values) between the phase of low-frequency signals (3–15 Hz in 1 Hz steps) and the amplitude of high-frequency signals (20–100 Hz) in 5 Hz steps. As discussed in prior work, the modulating frequency must be lower than the amplitude-modulated frequency (Berman et al., 2012).

Population statistics was performed on each regional location's set of resultant comodulograms using *t*-tests for each frequency pair. Given the large number of comparisons across the comodulograms for each regional location, these results were familywise corrected using suprathreshold clustering and bootstrapping (Nichols and Holmes, 2002). Regional location comodulograms that demonstrated clusters of significantly altered PAC in ASD subsequently underwent additional processing to assess any observed diagnosis-related perturbations. For each frequency pair where significant group differences were observed, Cohen's *d* statistic of effect size was calculated.

The whole-brain pattern of alpha to low-gamma-band PAC group differences was also examined. Theta (4–8 Hz), low-alpha (9–12 Hz), and high-alpha (12–14 Hz) phase bands were chosen for whole-brain analysis based on visual inspection of the within-region comodulograms and to avoid spectral edge effects. The T-score representing the regional PAC group differences was plotted on a template brain (the ICBM152 average brain) and subsequently masked by significance at $p < 0.05$.

Further analyses required a single MI value per participant at each regional location corresponding to the frequency pairs most altered in ASD. For each region, the frequency pairing that exhibited the greatest absolute Cohen's *d* statistic within the group-level regional comodulogram was determined. Subsequently, for each subject, the MI_{Max} value was calculated as the mean from a 3×3 frequency pairing square region of the comodulgram centered on the frequency pairing that exhibited the greatest absolute Cohen's *d* statistic.

To assess the relationship between the observed clusters of altered low-gamma PAC in ASD and any potential concomitant underlying power alterations, linear regressions were performed. The MI_{Max} restricted to low-gamma amplitudes was computed to attain a single MI value per subject for each cluster within regional group-level comodulograms that demonstrated significantly altered low-gamma PAC between ASD and TD. Subsequently, Bonferroni corrected linear regressions separately examined each regional location's MI values modeled by the main effects of diagnosis, the underlying canonical modulation power, as well as their interaction.

The maturational trajectory of PAC was of interest both in typical development and in the developmental disorder ASD. To examine the maturational trajectory, the mean MI_{Max} values were computed and included as repeated measures in an analysis of covariance (ANCOVA) with the fixed effect of diagnosis, as well as the covariate of age, and interactions of age by location and diagnosis by location. Sidak multiple comparison correction was implemented to avoid false positives. To ensure that the results of this original repeated-measures ANCOVA were not biased toward ASD, due to the greater number of participants with ASD as opposed to TD participants, an analogous repeated-measures ANCOVA was performed separately for each diagnostic group. Subsequently, Pearson's correlations separately examined the relationship between age and MI_{Max} values from the frequency pairing that demonstrated the highest (temporal posterior right [TPR] 8 Hz coupled to 50 Hz), as well as the most negative (central midline [CM] 11 Hz coupled to 45 Hz), group effect sizes.

To examine the relationship between PAC estimates and ASD symptom severity, Pearson's correlations were performed between SRS T-score and PAC estimates. SRS T-scores from both individuals with ASD and their TD counterparts were included in these analyses to interrogate the entire range of SRS scores. For these analyses, the frequency pairing that demonstrated the most positive (TPR 8 Hz coupled to 50 Hz), as well as the most negative (CM 11 Hz coupled to 45 Hz), group effect sizes was again selected to reduce the number of multiple comparisons.

Further examination of the distribution of MI values indicated potential noise floor confounds during the aforementioned correlational analyses. As such, the following bootstrapping procedure that retains the spectral structure of the original signal was undertaken to estimate the noise floor. After filtering the recorded signal into a higher frequency and lower frequency signal, each higher frequency signal was divided into 10 segments. This segmented higher frequency signal was then recombined 1000 times in a random time order, and MI values generated for the coupling between this artificial higher frequency signal and the native lower frequency signal's phase. This artificial MI represented the PAC present in a randomly coupled and scrambled signal. This generation of noise floor value distributions was repeated for every frequency pair. Subsequently, these values were formed into a matrix that represented the distribution of noise floor values over the entire comodulogram, referred to as the noise comodulogram. These resultant noise floor values were then compared between diagnostic groups and were found to be not significantly different ($p > 0.05$). The original correlational analyses comparing SRS T-score to PAC estimates were repeated, with MI_{Max} values less than the noise floor discarded. To confirm the presence of the observed correlation between SRS T-score with PAC estimates values, a skipped Pearson's correlation (Wilcox, 2004) with subsequent bootstrapping of correlation coefficients was performed after rejecting outliers using the interquartile range rule. This conformational analysis was performed using the robustcorrtool toolbox (Pernet et al., 2012). As the effect of age was a potential confound in the observed correlation between SRS T-score and TPR PAC, hierarchical regressions tested the relationship between SRS and age to PAC.

Quality assurance

Recent work has demonstrated that at least of 60 sec of data are required to obtain stable PAC estimates when using variable bandwidth filters (Berman et al., 2015). As such, all participants were required to have at least 70 sec of artifact-free RS data to ensure stable PAC estimates. In addition, participants' data were removed from analyses if they were observed to be an outlier (defined as 3 standard deviations [SDs] from their diagnostic age-corrected group mean) on RS power or PAC. As a result of these quality assurance measures, three TD controls and nine children with ASD were

excluded from the final study cohort. There was no significant difference between diagnostic groups in the amount of artifact-free data for the remaining subjects (TD = 170.52 s ± 81.61 [mean ± SD], ASD = 159.98 s ± 75.56 [mean ± SD]; $p > 0.05$). Finally, frequency pairs demonstrating significant group differences on the edges of the comodulogram were disregarded as these regions are more sensitive to noise contamination (Berman et al., 2015).

Demographics

Table 1 summarizes the study population after all quality assessment procedures. The analysis included 119 children with ASD (9.98 ± 2.16 years old [mean ± SD]) and 47 TD children (9.38 ± 2.25 years old [mean ± SD]), with no group difference in age ($p > 0.05$). In addition, the diagnostic groups did not differ on age distribution (two-sample Kolmogorov–Smirnov test, $p > 0.05$). Fourteen children with ASD and 15 TD children were female ($\chi^2 = 9.90$, $p < 0.01$). As expected, children with ASD demonstrated higher SRS T-scores than TD children (TD = 43.57 ± 5.26 [mean ± SD]; ASD = 75.12 ± 12.40 [mean ± SD]; $p < 0.001$; SRS values unavailable for three TD children and six children with ASD). Children with ASD demonstrated lower GAI than their TD counterparts, but the group difference was less than 1 SD (TD = 115.14 ± 14.50 [mean ± SD]; ASD = 103.71 ± 18.53 [mean ± SD]; $p < 0.05$; GAI values unavailable for four TD children and seven children with ASD).

Table 1. Study Population Demographics and Age Distribution Within Diagnostic Groups

	TD	*ASD*
	Count	
Study population demographics		
N	47	119
Female (*N*)	15	14
	Mean (SD)	
Age	9.38 (2.25)	9.98 (2.16)
GAI	115.14 (14.50)	103.71 (18.53)
SRS	43.57 (5.26)	75.12 (12.40)
	Age (years old)	
	TD	*ASD*
Study population age distribution		
Minimum	4.08	5.94
Maximum	14.07	15.65
	Count	
4–8 Years old	12	20
8–12 Years old	30	81
12–16 Years old	5	18

Study population demographics—first section: the number of participants (*N*), as well as number of female participants (Female *N*), included in the study after all quality assessment procedures for the TD and ASD cohorts. Study population demographics—second section: mean (and SD) age (first row), GAI score (second row), and SRS score (third row) for the TD and ASD cohorts. Study population age distribution—first section: minimum (first row) and maximum (second row) age for the TD and ASD cohorts. Study population age distribution—second section: number of subjects, ages between 4 and 8 years (first row), between 8 and 12 years (second row), and between 12 and 16 years (third row), for TD and ASD cohorts.

ASD, autism spectrum disorder, GAI, General Ability Index; *N*, count; SD, standard deviation; SRS, Social Responsiveness Scale; TD, typically developing.

Results

For a summary of significant observations, see Table 2.

RS bandpassed power

Results of the RS bandpassed power analyses are presented in Figure 2. Individuals with ASD demonstrated greater alpha and theta power in posterior and parietal regions than their TD counterparts (OpM, parietal left [PL], parietal midline [PM], parietal right [PR], temporal posterior left [TPL], and TPR regions, each $p < 0.01$), findings consistent with Cornew et al. (2012) and Edgar et al. (2015b). Individuals with ASD exhibited greater parietal delta power than their TD counterparts (PL, PM, PR all at least $p < 0.05$). Greater alpha, theta, and delta power for ASD was observed in right-hemisphere anterior temporal lobe (temporal anterior right, all at least $p < 0.05$). Greater delta power was also observed for ASD in the frontal medial pole location (frontopolar midline, $p < 0.01$).

In contrast, individuals with ASD demonstrated lower alpha and theta power at select frontal and central sources compared with TD. Alpha power was decreased at frontal left (FL), frontal midline (FM), and CM ($p < 0.001$ for all). Individuals with ASD demonstrated less theta power at FM ($p < 0.01$) as well as CM ($p < 0.001$) sources.

Resting-state PAC

Each location's comodulogram was examined for clusters of altered PAC in ASD versus TD. Spatially heterogeneous, yet specific, regions of altered PAC were observed. Specifically, the CM location demonstrated a cluster of greater PAC in ASD in the 9–11 Hz coupled to 25–55 Hz frequency pairings ($p < 0.05$). In addition, clusters of greater PAC in ASD compared with TD were observed in ASD in frontal locations (FL = 8–9 Hz coupled to 75–85 Hz frequency pairings; frontal right = 7 Hz coupled to 65–75 Hz frequency pairings; FM = 11 Hz coupled to 90–95 Hz frequency pairings, all $p < 0.05$).

Midline parietal and also right-hemisphere central comodulograms demonstrated less PAC in ASD than TD (PM = 4–6 Hz coupled to 45–50 Hz frequency pairings as well as 5–6 Hz coupled to 70–80 Hz frequency pairings; central right [CR] = 5–14 Hz coupled to 30–65 Hz clusters). In addition, the posterior temporal lobe in both hemispheres demonstrated two clusters of altered PAC between ASD and TD, one in the theta to low-gamma region (TPL = 6–7 Hz coupled to 25–55 Hz frequency pairings; TPR = 4–9 Hz coupled to 30–55 Hz frequency pairings) and one in the high-alpha region (TPL = 12–14 Hz coupled to 25–40 Hz frequency pairings; TPR = 11–14 Hz coupled to 25–55 Hz frequency pairings).

Subsequently, the spatial pattern of low-gamma PAC group differences was examined. Alpha to low-gamma and theta to

Table 2. Summary of Significant Observations Within the Current Study

	Posterior, parietal	*TAR*	*Frontal, central*
Resting power			
Delta	ASD>TD	ASD>TD	ASD>TD
Theta	ASD>TD	ASD>TD	TD>ASD
Alpha	ASD>TD	ASD>TD	TD>ASD
Beta	—	—	—
Low-gamma	—	—	—
High-gamma	—	—	—
	Medial		*Lateral*
Low-gamma PAC			
Theta	—		TD>ASD
Alpha	ASD>TD		TD>ASD
	Medial (CM) finding		*Lateral (TPR) finding*
Correlation of PAC estimates with SRS T-score			
Pearson's correlation	Positive correlation		Negative correlation
Pearson's correlation of those above floor noise	Positive correlation		Negative correlation

CM, central midline; PAC, phase–amplitude coupling; TAR, temporal anterior right; TPR, temporal posterior right.

low-gamma regions of the comodulograms were of particular interest due to previous reports of abnormal alpha to low-gamma RS PAC in children with ASD (Berman et al., 2015). Alterations in PAC appeared in multiple locations (Fig. 3). TPR, TPL, and CR locations demonstrated less theta and alpha to low-gamma PAC in ASD than TD (blue regions; all $p<0.05$). Conversely, CM demonstrated greater alpha to low-gamma PAC in ASD than TD (red regions; all $p<0.05$), findings consistent with the earlier report (Berman et al., 2015). Of note, the PM location did not demonstrate PAC group differences, most likely due to the limited size of the cluster observed in the comodulogram-based analysis.

The relationship of the observed theta and alpha to low-gamma PAC alterations to underlying power was of interest. Linear models interrogated the theta and alpha to low-gamma PAC clusters observed in TPR, TPL, CM, and CR comodulograms against diagnosis, underlying modulation power, as well as their interaction. No main effect of modulation power or the interaction with diagnosis was significant after Bonferroni correction ($ps>0.10$).

Maturation of PAC

Maturation of PAC estimates across locations was examined. A Sidak-corrected repeated-measures ANCOVA demonstrated the expected significant interaction of location by diagnosis, $F(6.02,981.55)=3.17$, Greenhouse–Geisser correction, $p<0.01$, which reflected that the MI_{Max} values were explicitly selected because they had the largest Cohen's d statistic. In addition, the main effect of location was significant, $F(6.02,981.55)=4.27$, Greenhouse–Geisser correction, $p<0.001$, and with central left (first) and OpM (second) containing the largest MI_{Max} values, and PL (first) and FM (second) containing the smallest MI values. There was no immediately apparent ordering to this distribution. The main effect of diagnosis was significant, $F(1,163)=4.33$, Greenhouse–Geisser correction, $p<0.05$, with ASD exhibiting lower low-gamma PAC than TD across all locations. The main effect of age, as well as the interaction of age by location, failed to reach significance ($ps>0.10$). When repeating this analysis separately for each diagnostic group, the main effect of age as well as the age by location interaction again failed to reach significance ($ps>0.10$).

To confirm this surprising lack of low-gamma PAC maturation, Pearson's correlations examined the relationship between age and the MI_{Max} values from the frequency pairings that demonstrated the most positive (TPR 8 Hz coupled to 50 Hz), as well as the most negative (CM 11 Hz coupled to 45 Hz), group effect sizes. TPR MI_{Max} values demonstrated no association with age when considering the total sample, as well as when examining each group (all $ps>0.05$, Bonferroni corrected) (Fig. 4). Similarly, CM MI_{Max} values demonstrated no association with age when considering the total sample or separate groups (all $ps>0.05$, Bonferroni corrected).

PAC and behavioral metrics

The relationship between PAC estimates and behavioral metrics was also evaluated. To reduce the number of comparisons, only the MI_{Max} values from the frequency pairing that demonstrated the most positive (TPR 8 Hz coupled to 50 Hz), as well as the most negative (CM 11 Hz coupled to 45 Hz), group effect sizes were examined. SRS T-scores from the full sample were included so as to interrogate the entire range of SRS scores. The TPR PAC estimate was negatively correlated with SRS T-score ($r=-0.23$, $p<0.01$). A positive correlation was observed between the CM MI_{Max} values and SRS T-score ($r=0.25$, $p<0.01$).

Inspection of the distribution of PAC estimates suggested a noise floor confound. To address this concern, the correlation analyses were repeated after removing participants with MI_{Max} values below the corresponding noise floor level. Seventy-eight children/adolescents (26 TD—55.32% of the original cohort, 52 ASD—43.70% of the original cohort)

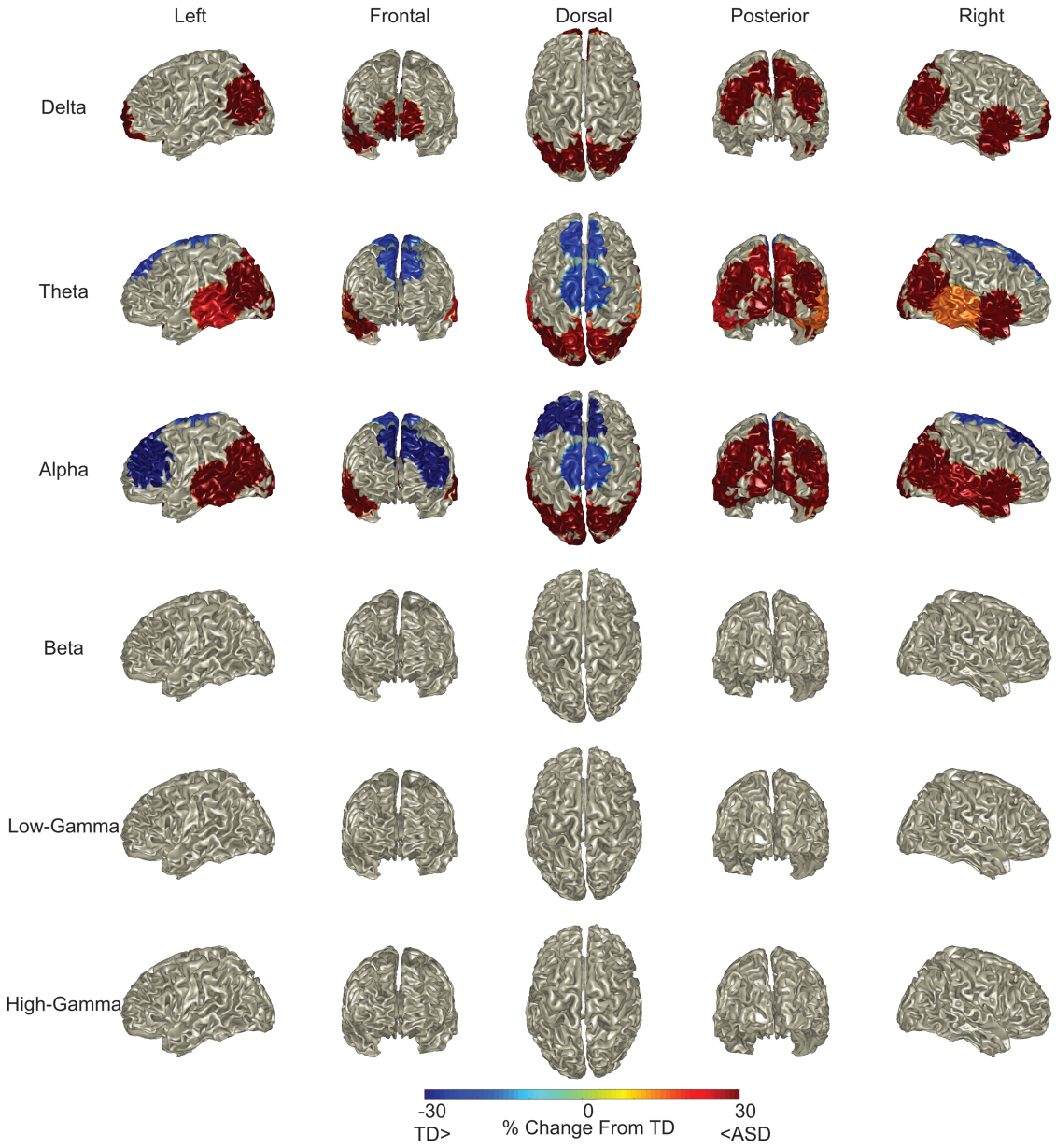

FIG. 2. RS power in different frequency bands by region. Individuals with ASD had less frontal/central alpha and theta power, as well as greater posterior alpha and theta power. Whole-brain (left column—left hemisphere surface of the brain, second to left column—frontal surface of the brain, middle column—dorsal surface of the brain, second to right column—posterior surface of the brain, right column—right hemisphere surface of the brain) visualization of ASD-induced alterations to RS power in the delta (top row), theta (second row), alpha (third row), beta (fourth row), low-gamma (fifth row), and high-gamma range (bottom row). Color on brain surface represents percent change from TD. Masking permits visualization only of regions with $p < 0.05$ for the pairwise comparison of diagnosis within the diagnosis by frequency band by source interaction (with Holm's correction for multiple comparisons). ASD, autism spectrum disorder; TD, typically developing. Color images are available online.

remained after noise floor-based rejection for the TPR PAC estimate analysis. Eighty-seven participants remained (18 TD—38.30% of the original cohort, 63 ASD—52.94% of the original cohort) after noise floor-based rejection for the CM PAC estimate analysis.

In these cohorts, the TPR PAC estimate was negatively correlated ($r = -0.35$, $p < 0.01$; Fig. 5A) and the CM PAC estimate was positively correlated ($r = 0.24$, $p < 0.05$; Fig. 5B) with SRS T-score. As these correlations may have been contaminated with outliers, skipped Pearson's correlations with subsequent bootstrapping of correlation coefficients were performed after rejecting outliers using the interquartile range rule, in accordance with Port et al. (2017a). The robust negative correlation between SRS T-score and the TPR PAC estimate was significant [$r = -0.35$, $t(66) = 3.29$, confidence intervals = -0.50 to -0.18). SRS T-score and the CM PAC estimates were significantly robustly positively correlated [$r = 0.24$, $t(80) = 2.23$, confidence intervals = 0.09–0.37].

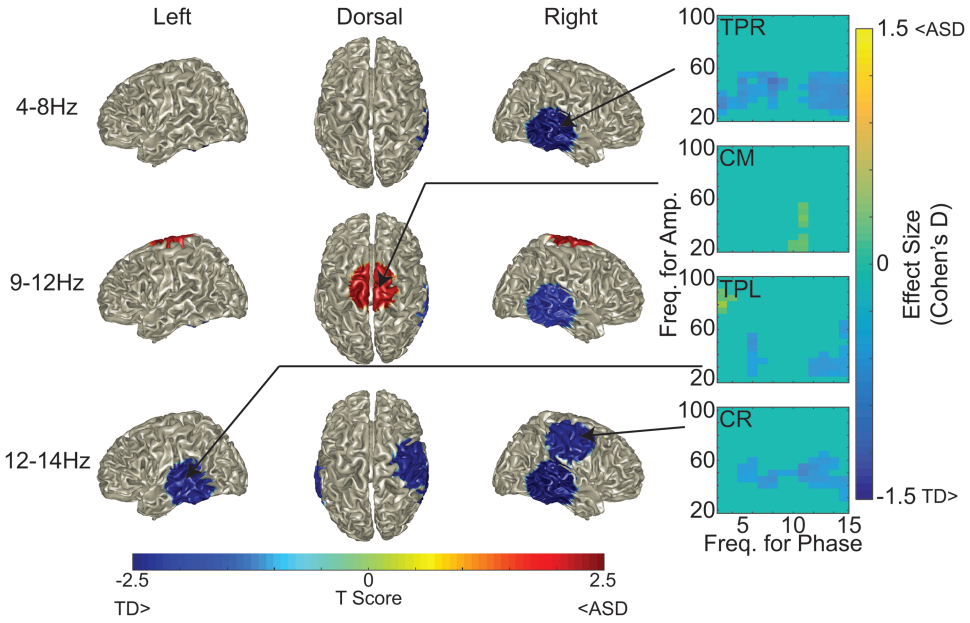

FIG. 3. Individuals with ASD demonstrated less right hemisphere, as well as greater midline, low-gamma PAC than TD. Whole-brain (left column—left hemisphere surface of brain, middle column—dorsal surface of brain, right column—right hemisphere surface of brain) visualization of ASD-induced alterations to average low-gamma PAC in the 4–8 Hz (top row), 9–12 Hz (middle row), and 12–14 Hz (bottom row) phase bands. Color on the brain surface represents the T-score of the ASD to TD comparison. Masking shows only locations with $p < 0.05$. Surrounding these surface depictions are the within-region comodulograms for the regions demonstrating significant ASD-induced altered low-gamma PAC. Comodulogram values are Cohen's *d* effect sizes. Color images are available online.

The effect of age on the correlation between SRS T-score and TPR PAC posed another potential confound. As such, the selected PAC estimate values were subsequently entered as the dependent variable in hierarchical regressions modeling age and SRS T-score. When entered first, age accounted for 1% of the variance in TPR PAC estimates ($p > 0.10$). When entered second, SRS T-scores accounted for an additional 13% of the variance in TPR PAC estimates (ΔR^2 $p <$ 0.01). For the corresponding hierarchical regression of CM PAC estimates, age accounted for 4% of the variance ($p >$ 0.05) and SRS T-scores accounted for an additional 5% of the variance (ΔR^2 $p < 0.05$).

For the reciprocal hierarchical regression, SRS T-scores accounted for 13% of the variance in TPR PAC estimates ($p < 0.01$) when entered first. Entered second, age accounted

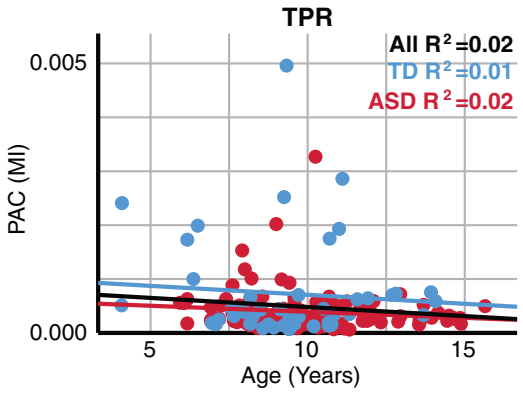

FIG. 4. TPR PAC did not demonstrate maturation. TPR PAC estimates (TPR MI_{Max}; MI; *y*-axis) did not change as a function of age (age; years old; *x*-axis). Blue markers represent TD and red markers ASD. Linear regression fits are displayed for TD (blue), ASD (red), and the total sample (black), with the corresponding R^2 in the top right corner. MI, modulation index. Color images are available online.

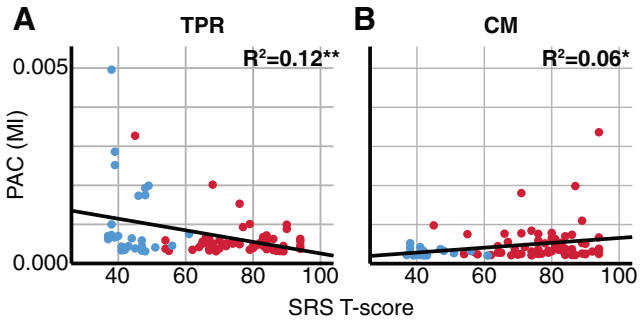

FIG. 5. PAC estimates are correlated with autism severity after removing subjects exhibiting PAC below noise floor levels. **(A)** TPR PAC estimates (TPR MI_{Max}; MI; *y*-axis) decreased with increased autism severity (SRS T-score; *x*-axis) after removing subjects exhibiting PAC below noise floor levels. **(B)** CM PAC estimates (CM MI_{Max}; MI; *y*-axis) increased with increased autism severity (SRS T-score; *x*-axis) after removing subjects exhibiting PAC below noise floor levels. Within each scatter plot, blue markers represent TD, red markers ASD, and the black line the linear regression fit for the total sample. $*p < 0.05$, $**p < 0.01$. SRS, Social Responsiveness Scale. Color images are available online.

for an additional 1% of the variance (ΔR^2 $p > 0.10$). Similarly, for the CM PAC estimates, SRS T-scores accounted for 6% of the variance ($p < 0.05$) when entered first. When entered second, age accounted for an additional 3% of the variance (ΔR^2 $p > 0.05$).

Discussion

Alterations in neural activity in individuals with ASD are well documented. Recently, the cross-frequency interactions in ASD have been studied, with both increased (Berman et al., 2015) and decreased (Khan et al., 2013; Mamashli et al., 2017; Seymour et al., 2018) PAC in ASD compared with TD. Inconsistencies in the pattern of PAC group differences across studies may be due to differences in task design (e.g., RS as opposed to visual stimuli) as well as the brain region(s) examined. Findings from the current study showed that PAC may be higher or lower in ASD depending on brain region. Findings also showed both negative and positive correlations between PAC and the SRS index of ASD severity, corresponding to the direction of the group PAC difference at each brain region. These findings support the Khan et al. (2013) finding of a correlation of ASD severity (ADOS) with PAC. Currently, it remains unclear what biological underpinnings or mechanisms account for the observed differential relationship between SRS score and medial (CM) or lateral (TPR) regional PAC.

Regionally specific alterations to theta and alpha RS power, as well as theta and alpha to low-gamma PAC, were observed in ASD. No group differences in RS gamma power were observed. Whereas alpha power was differentially altered in ASD compared with TD in CM versus lateral posterior sources, linear regressions did not show a modulatory effect of alpha power on the MI values. This lack of modulation of low-gamma amplitude by the power of the underlying modulation frequency suggests that a different biological mechanism underlies the ASD abnormalities observed for low-frequency power versus PAC.

PAC examines interactions across frequency bands, enabling investigation of how long-range alpha networks modulate local cortical gamma activity. Alterations to gamma-band activity in individuals with ASD have been well documented (Edgar et al., 2015c; Port et al., 2016; Wilson et al., 2007). Children with ASD have abnormal development of long-range white matter microstructure network connectivity (Berman et al., 2016; McLaughlin et al., 2018; Roberts et al., 2013). The above suggests that white matter abnormalities may account for the abnormal PAC observed in the present study.

Spatially heterogeneous alterations to theta and alpha to low-gamma PAC were observed in ASD. CM RS alpha to gamma PAC was increased in ASD relative to TD, mirroring the Berman et al. (2015) findings from a dorsal medial source. In addition, decreased lateral RS theta and alpha to low-gamma PAC in individuals with ASD was also observed, with this pattern akin to the Khan et al. (2013) findings from ventral and more lateral source. As such, the current findings suggest that the directionality of ASD alpha to low-gamma PAC alternations may be attributed to the brain region examined as opposed to task design. Although the present whole-brain PAC analyses were not corrected for multiple comparisons, the spatial pattern of PAC changes demonstrated greater spatial coherence than expected due to false positives. In addition, it is unlikely that a single generator is producing the observed spatial pattern due to (1) the distance between regional sources, and (2) the presence of increased as well as decreased regions of low-gamma PAC for individuals with ASD than TD.

To provide context to the observed PAC alterations, RS power within canonical frequency bands was also investigated. Previous studies disagree about the directionality of RS power alterations in ASD (Rojas and Wilson, 2014), possibly due to methodological inconsistencies (Maxwell et al., 2015). This study observed that individuals with ASD demonstrated greater posterior and parietal alpha as well as theta power compared with their TD counterparts, in accordance with several previous studies (Cornew et al., 2012; Edgar et al., 2015b).

The factors accounting for alterations to RS power and PAC are likely complex, with individuals with ASD exhibiting numerous neurobiological alterations, ranging from protein levels (Fatemi et al., 2002, 2014; Shimmura et al., 2013) to long-range white matter tracts (Berman et al., 2016; Iidaka et al., 2012; Nagae et al., 2012; Wolff et al., 2012). Often, such changes are regionally specific. Moreover, ASD is usually conceptualized as a brain-wide disorder. Within this setting, laboratories often focus on particular brain regions/structures due to an involvement of the brain regions in one or more of the examined behaviors. Against this complex background of neurobiological alterations in ASD, it is unsurprising that oscillatory activity differs from TD individuals, both with respect to frequency band and spatial pattern. These neurophysiological alterations are of interest, as previous studies have linked power alterations in alpha (Cornew et al., 2012; Edgar et al., 2015b) and gamma (Maxwell et al., 2015) to ASD severity. Although the biological underpinnings of oscillatory activities in healthy subjects are increasingly understood (Wang, 2010), how the observed neurobiological alterations in ASD affect these neural mechanisms remains unclear even within a single source and frequency band, let alone in conjunction.

Abnormal maturation of white matter and electrophysiology in ASD have been repeatedly observed (Belmonte et al., 2004; Cornew et al., 2012; Courchesne et al., 2004, 2007; Hazlett et al., 2012; Port et al., 2016, 2017a; Roberts et al., 2013; Tierney et al., 2012). As such, the maturation of PAC in the present cohort was of direct relevance. Repeated-measures ANCOVAs demonstrated no significant maturational change in regional PAC estimates. Similar results were observed within each diagnostic group. A lack of maturation of PAC conflicts with Cho et al. (2015), who reported increasing PAC with age. Of note though, maturation of PAC is likely not unitary; whereas alpha to high-gamma PAC may mature over time, low-gamma may not (Mamashli et al., 2018). Additional studies examining the effect of maturation on PAC are needed.

Conclusions

Individuals with ASD demonstrated regionally specific heterogeneous alterations to RS power as well as PAC. Commensurate with the spatial pattern of PAC abnormalities,

low-gamma PAC estimates were related to ASD severity, with the directionality of the relationship depending on brain region.

Acknowledgments

The authors thank John Dell, Peter Lam, and Rachel Golembski for technical assistance. This study was supported, in part, by NIH grant 5T32MH019112-27 (R.G.P.), K01MH096091 (J.I.B.), R21MH110869 (J.I.B.), NIH grant R01MH107506, NICHD grant R01HD093776 (J.C.E.), R21MH098204 (J.C.E.), R01HD073258 (coprincipal investigator T.P.L.R.), R01DC008871 (T.P.L.R.), U54 HD086984 (Intellectual and Developmental Disabilities Research Center Group at the CHOP), and Award number P30HD026979 from the Eunice Kennedy Shriver National Institute of Child Health and Human Development of the NIH. Dr. Roberts additionally acknowledges the Oberkircher Family for the Oberkircher Family Chair in Pediatric Radiology at the CHOP. Finally, the authors thank Mrs. Allison M. Port for her tireless efforts on this article.

Author Disclosure Statement

Dr. Berman discloses consulting agreements with McGowan Associates. Dr. Roberts discloses consulting arrangements with Prism Clinical Imaging, Siemens Medical Solutions, Elekta Oy, Guerbet, Johnson and Johnson (Janssen division) CTF, Ricoh, Spago Nanomedicine, Avexis Inc., and Acadia Pharmaceuticals. Dr. Roberts and Dr. Edgar also own intellectual property relating to the potential use of electrophysiological markers for treatment planning in clinical ASD. All other authors declare no consulting arrangements or business interests. As such, the authors have no commercial associations that might create a conflict of interest in connection with this work. These data were previously presented, in part, at IMFAR 2018, and a subset of the subjects RS PM PAC was reported in Berman et al. (2015) and RS bandpassed power in Cornew et al. (2012).

References

American Psychiatric Association. 2013. *Diagnostic and Statistical Manual of Mental Disorders*. Washington, DC: American Psychiatric Publishing, Inc.

Belmonte MK, Allen G, Beckel-Mitchener A, Boulanger LM, Carper RA, Webb SJ. 2004. Autism and abnormal development of brain connectivity. J Neurosci 24:9228–9231.

Berman JI, Edgar JC, Blaskey L, Kuschner ES, Levy SE, Ku M, et al. 2016. Multimodal diffusion-MRI and MEG assessment of auditory and language system development in autism spectrum disorder. Front Neuroanat 10:30.

Berman JI, Liu S, Bloy L, Blaskey L, Roberts TP, Edgar JC. 2015. Alpha-to-gamma phase-amplitude coupling methods and application to autism spectrum disorder. Brain Connect 5:80–90.

Berman JI, McDaniel J, Liu S, Cornew L, Gaetz W, Roberts TP, Edgar JC. 2012. Variable bandwidth filtering for improved sensitivity of cross-frequency coupling metrics. Brain Connect 2:155–163.

Buzsaki G, Wang XJ. 2012. Mechanisms of gamma oscillations. Annu Rev Neurosci 35:203–225.

Canolty RT, Edwards E, Dalal SS, Soltani M, Nagarajan SS, Kirsch HE, et al. 2006. High gamma power is phase-locked to theta oscillations in human neocortex. Science 313: 1626–1628.

Cho RY, Walker CP, Polizzotto NR, Wozny TA, Fissell C, Chen CM, Lewis DA. 2015. Development of sensory gamma oscillations and cross-frequency coupling from childhood to early adulthood. Cereb Cortex 25:1509–1518.

Constantino J, Gruber CP. 2012. *Social Responsiveness Scale*. Los Angeles, CA: Western Psychological Services.

Cornew L, Roberts TP, Blaskey L, Edgar JC. 2012. Resting-state oscillatory activity in autism spectrum disorders. J Autism Dev Disord 42:1884–1894.

Courchesne E, Pierce K, Schumann CM, Redcay E, Buckwalter JA, Kennedy DP, Morgan J. 2007. Mapping early brain development in autism. Neuron 56:399–413.

Courchesne E, Redcay E, Kennedy DP. 2004. The autistic brain: birth through adulthood. Curr Opin Neurol 17:489–496.

Edgar JC, Fisk IV CL, Berman JI, Chudnovskaya D, Liu S, Pandey J, et al. 2015a. Auditory encoding abnormalities in children with autism spectrum disorder suggest delayed development of auditory cortex. Mol Autism 6:69.

Edgar JC, Heiken K, Chen YH, Herrington JD, Chow V, Liu S, et al. 2015b. Resting-state alpha in autism spectrum disorder and alpha associations with thalamic volume. J Autism Dev Disord 45:795–804.

Edgar JC, Khan SY, Blaskey L, Chow VY, Rey M, Gaetz W, et al. 2015c. Neuromagnetic oscillations predict evoked-response latency delays and core language deficits in autism spectrum disorders. J Autism Dev Disord 45:395–405.

Fatemi SH, Halt AR, Stary JM, Kanodia R, Schulz SC, Realmuto GR. 2002. Glutamic acid decarboxylase 65 and 67 kDa proteins are reduced in autistic parietal and cerebellar cortices. Biol Psychiatry 52:805–810.

Fatemi SH, Reutiman TJ, Folsom TD, Rustan OG, Rooney RJ, Thuras PD. 2014. Downregulation of GABAA receptor protein subunits alpha6, beta2, delta, epsilon, gamma2, theta, and rho2 in superior frontal cortex of subjects with autism. J Autism Dev Disord 44:1833–1845.

Fatemi SH, Reutiman TJ, Folsom TD, Thuras PD. 2009. GABA(A) receptor downregulation in brains of subjects with autism. J Autism Dev Disord 39:223–230.

Fonov VS, Evans AC, McKinstry RC, Almli CR, Collins DL. 2009. Unbiased nonlinear average age-appropriate brain templates from birth to adulthood. Neuroimage 47:S102.

Gaetz W, Bloy L, Wang DJ, Port RG, Blaskey L, Levy SE, Roberts TP. 2014. GABA estimation in the brains of children on the autism spectrum: measurement precision and regional cortical variation. Neuroimage 86:1–9.

Gandal MJ, Sisti J, Klook K, Ortinski PI, Leitman V, Liang Y, et al. 2012. GABAB-mediated rescue of altered excitatory-inhibitory balance, gamma synchrony and behavioral deficits following constitutive NMDAR-hypofunction. Transl Psychiatry 2:e142.

Gogolla N, Leblanc JJ, Quast KB, Sudhof TC, Fagiolini M, Hensch TK. 2009. Common circuit defect of excitatory-inhibitory balance in mouse models of autism. J Neurodev Disord 1:172–181.

Gotham K, Pickles A, Lord C. 2009. Standardizing ADOS scores for a measure of severity in autism spectrum disorders. J Autism Dev Disord 39:693–705.

Grice SJ, Spratling MW, Karmiloff-Smith A, Halit H, Csibra G, de Haan M, Johnson MH. 2001. Disordered visual processing and oscillatory brain activity in autism and Williams syndrome. Neuroreport 12:2697–2700.

Harada M, Taki MM, Nose A, Kubo H, Mori K, Nishitani H, Matsuda T. 2011. Non-invasive evaluation of the GABAergic/glutamatergic system in autistic patients observed by MEGA-editing proton MR spectroscopy using a clinical 3 tesla instrument. J Autism Dev Disord 41:447–454.

Hazlett HC, Poe MD, Lightbody AA, Styner M, MacFall JR, Reiss AL, Piven J. 2012. Trajectories of early brain volume development in fragile X syndrome and autism. J Am Acad Child Adolesc Psychiatry 51:921–933.

Hoechstetter K, Bornfleth H, Weckesser D, Ille N, Berg P, Scherg M. 2004. BESA source coherence: a new method to study cortical oscillatory coupling. Brain Topogr 16:233–238.

Hussman JP. 2001. Suppressed GABAergic inhibition as a common factor in suspected etiologies of autism. J Autism Dev Disord 31:247–248.

Iidaka T, Miyakoshi M, Harada T, Nakai T. 2012. White matter connectivity between superior temporal sulcus and amygdala is associated with autistic trait in healthy humans. Neurosci Lett 510:154–158.

Just MA, Cherkassky VL, Keller TA, Minshew NJ. 2004. Cortical activation and synchronization during sentence comprehension in high-functioning autism: evidence of underconnectivity. Brain 127(Pt 8):1811–1821.

Khan S, Gramfort A, Shetty NR, Kitzbichler MG, Ganesan S, Moran JM, et al. 2013. Local and long-range functional connectivity is reduced in concert in autism spectrum disorders. Proc Natl Acad Sci U S A 110:3107–3112.

Kopell NJ, Gritton HJ, Whittington MA, Kramer MA. 2014. Beyond the connectome: the dynome. Neuron 83:1319–1328.

Le Couteur A, Lord C, Rutter M. 2003. *The Autism Diagnostic Interview—Revised (ADI-R)*. Los Angeles, CA, Western Psychological Services.

Lord C, Risi S, Lambrecht L, Cook JEH, Leventhal BL, DiLavore PC, et al. 2000. The autism diagnostic observation schedule—generic: a standard measure of social and communication deficits associated with the spectrum of autism. J Autism Dev Disord 30:205–223.

Lord C, Rutter M, DiLavore PC, Risi S, Gotham K, Bishop SL. 2012. *Autism Diagnostic Observation Schedule Second Edition (ADOS- 2) Manual*. Torrance, CA: Western Psychological Services.

Mamashli F, Khan S, Bharadwaj H, Losh A, Pawlyszyn SM, Hamalainen MS, Kenet T. 2018. Maturational trajectories of local and long-range functional connectivity in autism during face processing. Hum Brain Mapp 39:4094–4104.

Mamashli F, Khan S, Bharadwaj H, Michmizos K, Ganesan S, Garel KA, et al. 2017. Auditory processing in noise is associated with complex patterns of disrupted functional connectivity in autism spectrum disorder. Autism Res 10: 631–647.

Maxwell CR, Villalobos ME, Schultz RT, Herpertz-Dahlmann B, Konrad K, Kohls G. 2015. Atypical laterality of resting gamma oscillations in autism spectrum disorders. J Autism Dev Disord 45:292–297.

McLaughlin K, Travers BG, Dadalko OI, Dean 3rd DC, Tromp D, Adluru N, et al. 2018. Longitudinal development of thalamic and internal capsule microstructure in autism spectrum disorder. Autism Res 11:450–462.

Nagae LM, Zarnow DM, Blaskey L, Dell J, Khan SY, Qasmieh S, et al. 2012. Elevated mean diffusivity in the left hemisphere superior longitudinal fasciculus in autism spectrum disorders increases with more profound language impairment. AJNR Am J Neuroradiol 33:1720–1725.

Nichols TE, Holmes AP. 2002. Nonparametric permutation tests for functional neuroimaging: a primer with examples. Hum Brain Mapp 15:1–25.

Nunez PL, Srinivasan R, Westdorp AF, Wijesinghe RS, Tucker DM, Silberstein RB, Cadusch PJ. 1997. EEG coherency: I: statistics, reference electrode, volume conduction, Laplacians, cortical imaging, and interpretation at multiple scales. Electroencephalogr Clin Neurophysiol 103:499–515.

Osipova D, Hermes D, Jensen O. 2008. Gamma power is phase-locked to posterior alpha activity. PLoS One 3:e3990.

Pernet CR, Wilcox R, Rousselet GA. 2012. Robust correlation analyses: false positive and power validation using a new open source matlab toolbox. Front Psychol 3:606.

Port RG, Edgar JC, Ku M, Bloy L, Murray R, Blaskey L, et al. 2016. Maturation of auditory neural processes in autism spectrum disorder—a longitudinal MEG study. Neuroimage Clin 11:566–577.

Port RG, Gaetz W, Bloy L, Wang DJ, Blaskey L, Kuschner ES, et al 2017a. Exploring the relationship between cortical GABA concentrations, auditory gamma-band responses and development in ASD: evidence for an altered maturational trajectory in ASD. Autism Res 10:593–607.

Port RG, Gajewski C, Krizman E, Dow HC, Hirano S, Brodkin ES, et al. 2017b. Protocadherin 10 alters gamma oscillations, amino acid levels, and their coupling; baclofen partially restores these oscillatory deficits. Neurobiol Dis 108: 324–338.

Port RG, Berman JI, Liu S, Featherstone RE, Roberts TPL, Siegel SJ. 2019. Parvalbumin cell ablation of NMDA-R1 leads to altered phase, but not amplitude, of gamma-band cross-frequency coupling. Brain 9:263.

R Core Team. 2018. *R: A Language and Environment for Statistical Computing*. Vienna: R Foundation for Statistical Computing.

Roberts TP, Lanza MR, Dell J, Qasmieh S, Hines K, Blaskey L, et al 2013. Maturational differences in thalamocortical white matter microstructure and auditory evoked response latencies in autism spectrum disorders. Brain Res 1537: 79–85.

Rojas DC, Wilson LB. 2014. Gamma-band abnormalities as markers of autism spectrum disorders. Biomark Med 8:353–368.

Rubenstein JLR, Merzenich MM. 2003. Model of autism: increased ratio of excitation/inhibition in key neural systems. Genes Brain Behav 2:255–267.

Rutter M, Bailey A, Lord C. 2003. *Social Communication Questionnaire (SCQ)*. Los Angeles, CA: Western Psychological Services.

Seymour RA, Rippon G, Gooding-Williams G, Schoffelen J-M, Kessler K. 2018. Dysregulated oscillatory connectivity in the visual system in autism spectrum disorder. bioRxiv 440586; DOI: https://doi.org/10.1101/440586.

Shimmura C, Suzuki K, Iwata Y, Tsuchiya KJ, Ohno K, Matsuzaki H, et al. 2013. Enzymes in the glutamate-glutamine cycle in the anterior cingulate cortex in postmortem brain of subjects with autism. Mol Autism 4:6.

Singmann H, Bolker B, Westfall J, Aust F. 2015. afex: Analysis of factorial experiments. R Package.

Tierney AL, Gabard-Durnam L, Vogel-Farley V, Tager-Flusberg H, Nelson CA. 2012. Developmental trajectories of resting EEG power: an endophenotype of autism spectrum disorder. PLoS One 7:e39127.

Tort AB, Komorowski R, Eichenbaum H, Kopell N. 2010. Measuring phase-amplitude coupling between neuronal oscillations of different frequencies. J Neurophysiol 104: 1195–1210.

Traub RD, Spruston N, Soltesz I, Konnerth A, Whittington MA, Jefferys JGR. 1998. Gamma-frequency oscillations: a neuronal population phenomenon, regulated by synaptic and intrinsic cellular processes, and inducing synaptic plasticity. Prog Neurobiol 55:563–575.

Traub RD, Whittington MA, Colling SB, Buzsaki G, Jefferys JG. 1996. Analysis of gamma rhythms in the rat hippocampus in vitro and in vivo. J Physiol 493(Pt 2):471–484.

Wang XJ. 2010. Neurophysiological and computational principles of cortical rhythms in cognition. Physiol Rev 90:1195–1268.

Wass S. 2011. Distortions and disconnections: disrupted brain connectivity in autism. Brain Cogn 75:18–28.

Wechsler D. 2003. *Wechsler Intelligence Scale for Children—Fourth Edition. Administration and Scoring Manual*. San Antonio, TX: Harcourt Assessment, Inc.

Wechsler D. 2014. *Wechsler Intelligence Scale for Children—Fifth edition (WISC-V): Technical and Interpretive Manual*. Bloomington, MN: Pearson Clinical Assessment.

Wilcox R. 2004. Inferences based on a skipped correlation coefficient. J Appl Stat 31:131–143.

Wilson TW, Rojas DC, Reite ML, Teale PD, Rogers SJ. 2007. Children and adolescents with autism exhibit reduced MEG steady-state gamma responses. Biol Psychiatry 62: 192–197.

Wolff JJ, Gu H, Gerig G, Elison JT, Styner M, Gouttard S, et al 2012. Differences in white matter fiber tract development present from 6 to 24 months in infants with autism. Am J Psychiatry 169:589–600.

Address correspondence to:
Jeffrey I. Berman
Department of Radiology
Lurie Family Foundations MEG Imaging Center
Children's Hospital of Philadelphia
3400 Civic Center Boulevard
Philadelphia, PA 19104

E-mail: bermanj@email.chop.edu